Antiviral Research 211 (2023) 105546

Contents lists available at ScienceDirect

Antiviral Research

journal homepage: www.elsevier.com/locate/antiviral

Spike-mediated viral membrane fusion is inhibited by a specific anti-IFITM2 monoclonal antibody

Anna Basile [a], Carla Zannella [b], Margot De Marco [a,c], Giuseppina Sanna [d], Gianluigi Franci [a], Massimiliano Galdiero [b], Aldo Manzin [d], Vincenzo De Laurenzi [c,e], Massimiliano Chetta [f], Alessandra Rosati [a,c,*], Maria Caterina Turco [a,c], Liberato Marzullo [a,c]

[a] Department of Medicine, Surgery and Dentistry "Schola Medica Salernitana", University of Salerno, Baronissi, SA, 84081, Italy
[b] Department of Experimental Medicine, University of Campania "Luigi Vanvitelli", Naples, 80138, Italy
[c] FIBROSYS s.r.l., University of Salerno, Baronissi, SA, 84081, Italy
[d] Department of Biomedical Sciences, University of Cagliari, Cittadella Universitaria, Monserrato, 09042, Italy
[e] Department of Innovative Technologies in Medicine and Dentistry, University of Chieti-Pescara, Chieti, Italy
[f] U.O.C. Medical and Laboratory Genetics, A.O.R.N, Cardarelli, Naples, 80131, Italy

ARTICLE INFO

Keywords:
IFITM2
SARS-CoV-2
Virus entry
Syncytia
Monoclonal antibody

ABSTRACT

The early steps of viral infection involve protein complexes and structural lipid rearrangements which characterize the peculiar strategies of each virus to invade permissive host cells. Members of the human immune-related interferon-induced transmembrane (IFITM) protein family have been described as inhibitors of the entry of a broad range of viruses into the host cells. Recently, it has been shown that SARS-CoV-2 is able to hijack IFITM2 for efficient infection. Here, we report the characterization of a newly generated specific anti-IFITM2 mAb able to impair Spike-mediated internalization of SARS-CoV-2 in host cells and, consequently, to reduce the SARS-CoV-2 cytopathic effects and syncytia formation. Furthermore, the anti-IFITM2 mAb reduced HSVs- and RSV-dependent cytopathic effects, suggesting that the IFITM2-mediated mechanism of host cell invasion might be shared with other viruses besides SARS-CoV-2. These results show the specific role of IFITM2 in mediating viral entry into the host cell and its candidacy as a cell target for antiviral therapeutic strategies.

1. Introduction

In early 2020, the severe acute respiratory syndrome coronavirus 2 (SARS-CoV-2), showed its exceptional contagiousness, and the World Health Organization (WHO) classified COVID-19, the SARS-CoV-2-related disease, as a global pandemic. Thereafter, the virus spread into more than 200 countries, with severe public health and economic consequences. From October 2020, the emergence of new strains has been linked to new pathogenic variants in the Spike viral protein (Korber et al., 2020) and the WHO proposed categorizing them as Variants of Interest (VOI) and Variants of Concern (VOC), the latter characterized by increased transmissibility and risk of hospitalizations or deaths (Forster et al., 2020; Galloway et al., 2021).

The scientific community greatly contributed to pandemic control by paving the way for the development of several safe and effective COVID-19 vaccines (Van Kerkhove, 2021) having a major impact on avoiding mortality and helping countries' economies return to normal (Ledford, 2022a). Now, we have left behind a two-year pandemic that continues to pose a serious threat to public health in the near future; indeed, emerging virus variants may not respond to current preventive and therapeutic measures that thus need rapid adjustments and reformulations. Hence, current strategies against SARS-CoV-2 are focused on the development of vaccines (Fiolet et al., 2022) or monoclonal antibodies, both targeted at viral determinants to neutralize the infectious agent (Chew et al., 2022). Conversely, an alternative strategy could exploit the neutralization of determinants on the host cell surface that modulate the viral entry (Jackson et al., 2021). In this respect, some of the new therapeutics were chosen for their ability to block human proteins rather than viral proteins that SARS-CoV-2 uses to infiltrate cells (Ledford, 2022b), and studies on host cell infection routes (Mulder, 2022; Baggen et al., 2021) can lead to an advancement in our knowledge of infection mechanisms triggered by SARS-CoV-2 and possibly by other viruses as well.

Among host cell proteins, IFITMs were previously described as viral

* Corresponding author. Department of Medicine, Surgery and Dentistry "*Schola Medica Salernitana*", University of Salerno, Baronissi, SA, 84081, Italy.
E-mail address: arosati@unisa.it (A. Rosati).

https://doi.org/10.1016/j.antiviral.2023.105546
Received 13 October 2022; Received in revised form 12 January 2023; Accepted 15 January 2023
Available online 18 January 2023

restriction factors able to confer basal and IFN-induced resistance to Influenza A virus, Flaviviruses (Brass et al., 2009) and human coronaviruses including SARS-CoV-1 (Huang et al., 2011). On the other hand, it has been recently reported that endogenous IFITM2 can also act as essential entry cofactor for the efficient infection and replication of SARS-CoV-2 in various types of human cells. In fact, it has been shown that IFITM2 mimicking peptides and/or commercially available anti-IFITM2 antibodies inhibit SARS-CoV-2 infection of human lung, heart and gut cells (Prelli Bozzo et al., 2021). Moreover, it has been reported that the efficient replication of several SARS-CoV-2 VOCs depend on the presence of IFITM2 onto the target cells, thus suggesting that IFITM2 might play a key role in viral transmission and pathogenicity (Nchioua et al., 2022).

Due to the similarities among the IFITM family members (Yánez et al., 2019), it is crucial to produce highly specific reagents (antibodies, peptides) in order to investigate the pathways in which IFITM proteins are engaged. The design of a monoclonal antibody capable of specifically binding the extracellular N-terminal domain of the IFITM2 protein is detailed in this report. This anti-IFITM2 monoclonal antibody was used to demonstrate the functional relevance of IFITM2 in SARS-CoV-2 Spike protein internalization and Spike-mediated cellular fusion: the antibody was proven to block these pathways and, as a result, the cytopathic effect of the virus. The antibody also inhibited the cytopathic activity of other viruses, namely HSV1-2 and RSV, thus suggesting, as a proof of principle, an analogous role of IFITM2 also in cell infection by other viruses. As a whole, these data support the validity of an antiviral strategy based on the properties of host cell molecules that allow viral infection.

2. Materials and methods

2.1. Virus strains

SARS-CoV-2 original strain (clinical isolate kindly donated by Hospital Lazzaro Spallanzani, Rome, Italy), SARS-CoV-2 Omicron BA.1 variant (clinical isolate, strain EPI_ISL_13398512), Herpes Simplex (HSV-1 and HSV-2)- HSV-1 (strain SC16) and HSV-2 (ATCC VR-34) were propagated in Vero E6 cell monolayers (Zannella et al., 2021). Respiratory Syncytial Virus (RSV)- Human Respiratory Syncytial Virus (RSV) strain A2 (ATCC VR-1540) was propagated in Vero-76 cell monolayers.

2.2. Cell lines

Cell lines supporting the multiplication of RNA and DNA viruses were the following: monkey kidney Vero- 76 (ATCC CRL 1587) or Vero E6 (ATCC CRL-1586), human laryngeal carcinoma HEp-2 (ATCC CCL-23), human cervical adenocarcinoma HeLa (ATCC CRM-CCL-2) and human lung adenocarcinoma Calu-3 (ATCC HTB-55). Cell cultures were grown following ATCC guidelines for culturing media and in a 37 °C incubator with a humidified atmosphere of 5% CO_2 in the air.

2.3. Antibody production

The murine monoclonal anti-IFITM2 5D11B9 anti-IFITM2 antibody and the recombinant 5D11B9 murine human IgG_4 chimera were produced by Genscript (Piscataway, NJ, USA). The unrelated murine mAb was provided both in murine IgG_{2b} or human IgG_4 format by Evitria (Zurich, CH).

2.4. Cell viability and apoptosis assays

Vero E6 (1×10^4/well) and Calu-3 (2×10^4/wel) cells were seeded into the 96-well plates and cultured overnight at 37 °C. The cells were then incubated with different concentrations of monoclonal antibody 5D11B9 (80, 40, 20, 10 and 5 μg/ml) or with an unrelated murine IgG_{2b} (60 μg/ml). Cisplatin (30 μM) was used as a known cytotoxic agent. After 48 h, the CCK-8 solution (Sigma aldrich, #96992) was added to each well following the manufacturer's instructions. After 1 h of incubation, the absorbance of each well was measured using a microplate reader (450 nm), after which the results were statistically analyzed. PBMCs freshly isolated from healthy donors by standard techniques were incubated with FITC- annexin-V and propidium iodide (PI) for 15 min in the dark. The assay was performed using FITC Annexin V Apoptosis Detection Kit with propidium iodide (PI) (BioLegend) according to the manufacturer's instructions. Apoptotic cells were determined by flow cytometry (FacsVerse, Becton Dickinson).

2.5. Confocal microscopy

Calu-3 cells were incubated for 2 h at 4 °C, then a recombinant mouse- Fc tagged SARS-CoV-2 S1 protein (ProSci, #97-092) was added for 1 h to cells with a recombinant 5D11B9 m/h IgG4 or with an unrelated human IgG_4. After one additional hour, cells were incubated at 37 °C and harvested after 5 and 30 min. At the end of treatments, cells were washed with PBS 1X and fixed by adding 3.7% formaldehyde and then permeabilized with 0.005% saponin in PBS 1X/BSA 3% for 30 min at RT. For Calu-3 cell surface membrane staining, cells were fixed with 3.7% formaldehyde and then immunostained with the 5D11B9 murine mAb overnight at 4 °C. Signals were detected by using AF55-conjugated secondary anti-mouse IgGs (SouthernBiotech, #1031-32) for 1 h at RT. Slides were then mounted with ProLong Mountant (Thermo Fisher, #P36930) as well as with DAPI to visualize nuclei and analyze them using a confocal laser scanning microscope (Leica SP5). Images were acquired in sequential scan mode by using the same acquisition parameters when comparing experimental and control material.

2.6. ELISA assay for anti-IFITMs antibodies

96-well microplates were coated overnight at 4 °C with peptides (see supplementary information) or proteins: recombinant human IFITM1 (Proteintech, #Ag2320), recombinant human IFITM2 (Proteintech, #Ag17917), recombinant human IFITM3 (Proteintech, Ag17864). Wells were washed (PBS 1X/0.1% Tween-washing buffer) and blocked (PBS 1X- 0.5% fish gelatin-blocking buffer) for 1 h at RT, then washed again five times and loaded with different concentrations of anti-IFITM2 5D11B9 mAb for 1h at RT. After further washing, plates were incubated for 30 min at RT with HRP- conjugated anti-mouse IgGs (Jackson ImmunoResearch, #115-035-003). A TMB solution was added to the wells and the chromogenic reaction was blocked by acidification with 0.5 M H_2SO_4. The optical density (O.D.) was measured at 450 nm.

2.7. FACS binding assays

Vero E6 or Calu-3 cells were harvested with Non-Enzymatic Cell Dissociation Solution (ATCC 30–2103) and incubated with binding buffer (PBS 1X/10% decomplemented FBS/0.1% NaN_3) and FcR Blocking Reagent (Miltenyi Biotec, 130-059-901) following the manufacturer's instructions. Then, cells (1×10^6/ml) were resuspended in binding buffer (15 min at 4 °C) and incubated with the anti-IFITM2 5D11B9 murine mAb in binding buffer (30 min at 4 °C). An unrelated murine mAb was used as negative control. Cells were then washed three times with washing buffer (PBS 1X/2% decomplemented FBS/0.1% NaN_3), centrifuged (10 min at 300 g) and signals were revealed by using a PE-conjugated anti-mouse IgG (Miltenyi Biotec, #130-097-950) in binding buffer (30 min at 4 °C). For Spike binding, a biotinylated recombinant SARS-CoV-2 Spike protein (R&D Systems, BT10549) was pre-incubated (30 min at RT) with neutralizing or non-neutralizing human sera samples in binding buffer and the mix added to cells (1×10^5 cells). Vero E6 cells were also pre-incubated with the anti-IFITM2 5D11B9 murine mAb in binding buffer (30 min at 4 °C). After 1 h of incubation at 37 °C, cells were washed three times with washing buffer and centrifuged (10 min at 300 g). The cell membrane bound Spike protein was

revealed by using a PE-Streptavidin (SouthernBiotech, #7100-09M) in binding buffer (30 min at 4 °C). Thereafter, cells were washed three times with washing buffer, centrifuged and resuspended in binding buffer for flow cytometry analysis. 7-AAD (BioLegend, #420404) was used for the exclusion of non-viable cells in flow cytometric assays.

2.8. GFP-Split fusion assay

For the GFP-split fusion assay, 1×10^5 suspended cells were separately transfected with 250 ng of DNA in Eppendorf 1.5 mL tubes under 900 rpm orbital shaking for 30 min at 37 °C, using TransitX2 reagent. Donor cells were transfected with 125 ng of pQCXIP-GFP1-10 (Addgene, #68715) and 125 ng pCMV14-3X-Flag-SARS-CoV-2 S (Addgene, #68716). Acceptor cells were transfected with 125 ng of pQCXIP-BSR-GFP11 (Addgene, #68716) and 125 ng of an empty vector. After transfection, cells were washed and resuspended in complete medium, mixed at a 1:1 ratio and plated (2×10^5 cells/well) in 24-well plates. After 8 h, cells were incubated with anti-IFITM2 5D11B9 murine mAb or with unrelated control. 20 h post-transfection, cells were trypsinized and analyzed by flow cytometry. 7-AAD was used for the exclusion of non-viable cells in flow cytometric assays.

2.9. Plaque assay

Cells were plated in 12-well plates (2×10^5 cells/well) and at 80% confluence were treated with anti-IFITM2 5D11B9 murine mAb or with the unrelated control, and simultaneously infected with the SARS-CoV-2 or HSVs (5×10^6 PFU/mL). After 2 h, plates were washed with PBS 1X and a mixture of 3% carboxymethylcellulose/10% FBS was added to the culture medium (1:3). After 48 h, the cytopathic effect was first observed under the microscope and then plates were treated with a staining solution (Crystal Violet 0.5%/Formaldehyde 4%). Plaques were counted under the microscope and the viral inhibition was calculated by comparison with the untreated control (no mAb) using the formula: 100 - [(treatments well plaques/infected control plaques) x 100].

2.10. Proximity Ligation assay

Calu-3 cells were trypsinized, centrifuged (5 min at 500 g) and incubated with the recombinant mouse- Fc tagged SARS-CoV-2 S1 protein in complete medium in presence of the anti-IFITM2 5D11B9 murine/human IgG_4 or with an unrelated human IgG_4. After 1 h at 4 °C, cells were incubated at 37 °C and harvested after 5 and 30 min. The Duolink In situ PLA Detection Reagent FarRed (Sigma-Aldrich, #DUO92013) was used for protein proximity detection. Briefly, Calu-3 were centrifuged and washed with PBS 1X and fixed (3.7% formaldehyde/PBS 1X) for 10 min. After two washes, the cells were permeabilized with 0.5% Triton/PBS 1X for 7 min and blocked in Blocking Solution at 37 °C for 1 h. Next, the cells were aliquoted in a 96-well V-bottom plate (1×10^5 cells/well) and then incubated for 1 h at 37 °C with anti-ACE-2 (abcam, #ab272690) or anti-Rab5a (R&D Systems, ab-108-c) diluted in Duolink Antibody Diluent (Sigma-Aldrich, #DUO82008). After washing (wash buffer A), cells were incubated with secondary antibodies conjugated with PLUS and MINUS probes (Sigma-Aldrich, anti-Mouse MINUS PLA, DUO92004 and anti-Rabbit PLUS PLA, DUO2002) for 1 h at 37 °C. After additional washings, cells were incubated with the ligase and then incubated with the polymerase following the manufacturer's instructions. After a final wash with wash buffer B, cells were resuspended and analyzed by flow cytometry.

2.11. RT-PCR

Total RNA was isolated using TRIzol reagent and quantified by measuring the absorbance at 260/280 nm (NanoDrop 2000). Total RNA was reverse transcribed to cDNA by 5X All-In-One RT MasterMix (Applied Biological Materials, #G592). A quantitative polymerase chain reaction was run using BrightGreen 2X qPCR MasterMix-No Dye (Applied Biological Materials, G892) and a CFX Thermal Cycler (Bio--Rad). Relative target Ct (the threshold cycle) values of the S and N genes were analyzed in respect to GAPDH. Relative mRNA levels were expressed using the $2^{-\Delta\Delta Ct}$ method.

2.12. Yield reduction assays

Hep-2 cells or Calu-3 cells (5×10^5/ml) were infected with RSV or SARS-CoV-2 (100 TCID50) respectively in maintenance medium and contemporary mAbs and compounds were tested. After 96 h at 37 °C and 5% CO2, each sample was harvested and stored at −80 °C. Samples were then diluted with serial passages, starting from 10^{-1} up to 10^{-10}. The titer of the virus-containing supernatant dilutions series was determined by the TCID50/ml end-point in Vero 76.

2.13. Software and statistical analysis

Graphs were realized by using Excel (Suite Office 365) and GraphPad Prism 8.0. Results are expressed as means ± SD. Data were analyzed by Student's t-test and p values < 0.05 were considered statistically significant.

3. Results

3.1. Design and binding characterization of a specific anti-IFITM2 mAb

The high similarity of the amino acid sequences of human IFITM2 and IFITM3 - and to a lesser extent also IFITM1 - posed a first challenging task in the selection of the immunogens able to produce efficient and specific monoclonal antibodies selectively targeting IFITM2. The sequence analyses and the available literature data (Weston et al., 2014; Sun et al., 2020; Bailey et al., 2013; Prelli Bozzo et al., 2021) prompted us to focus the search on IFITM2 and IFITM3 N-Terminal Domains (NTD). The sequence analysis allowed the identification of a short sequence segment encompassing the highest number of unmatching amino acids that was selected as immunogen for mice's standard immunization procedures (Fig. 1A). The screening of hybridomas led to the identification of the clone 5D11B9 as the best performing clone in IFITM2 selective recognition. To test 5D11B9 mAb binding performance, IFITM2 or IFITM3 peptides, IFITM recombinant human proteins 1–3 were used as ligands in indirect ELISA tests. The results depicted in Fig. 1B show the selectivity of 5D11B9 mAb towards both IFITM2 peptide and full length human IFITM2 recombinant protein. Western Blot analysis on recombinant IFITM2 and IFITM3 NTDs confirmed this result (Fig. S1-panel A). The compared performances of other anti-IFITM2 commercial antibodies showed their cross reactivity against IFITM3 and none of them was able to bind the immunogen used to produce the 5D11B9 mAb (IFITM2 peptide) (Fig. S1-panel B). To test the binding of 5D11B9 anti-IFITM2 mAb to the NTD domain of plasma membrane-associated IFITM2, Vero E6 and Calu-3 cells were challenged with the antibody and analyzed by flow cytometry. Vero E6 and Calu-3 cells have been widely used as cellular models for SARS-CoV-2 in *in vitro* studies due to their susceptibility to the virus and the endogenous expression of the proteins ACE2 and TMPRSS2 on the plasma membrane (Lee et al., 2022; Shang et al., 2020). The cytofluorimetric analysis showed that the 5D11B9 mAb was able to bind the cell surface of both cell lines in a dose-dependent manner (Fig. 1C). These data also support a type III transmembrane topology for plasma membrane-associated IFITM2, characterized by the cell surface exposure of both N- and C-termini (NTD and CTD), respectively linked to two antiparallel transmembrane domains (TM1 and TM2) and connected to a short cytosolic inner loop (CIL). (Sun et al., 2020) Confocal microscopy carried out on non-permeabilized Calu-3 cells (Fig. 1D) confirmed the mAb binding on cell membrane and the signal specificity was verified by challenging the binding with competing IFITM2 and IFITM3 peptides

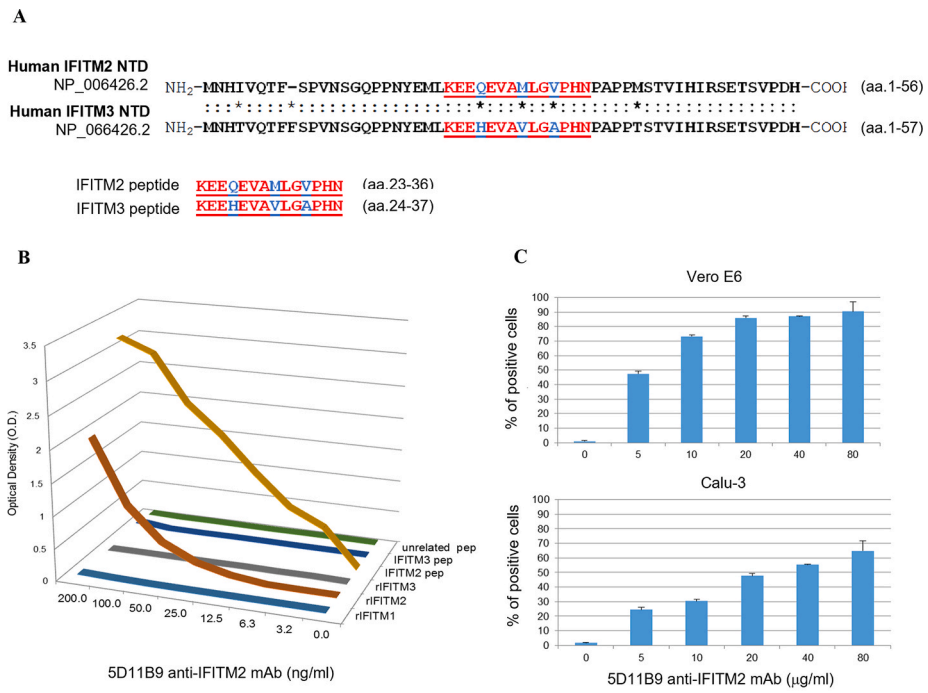

Fig. 1. Design and binding characterization of a specific anti-IFITM2 mAb.
A- Analysis of the N-Terminal (NTD) sequences of IFITM2 and IFITM3 and selection of short sequence stretches encompassing the highest number of amino acid substitutions to synthesize oligopeptides for mouse immunization. The sequence alignment and antigen sequences used to immunize the mice are displayed. **B-** IFITM2 peptide, IFITM3 peptide, an unrelated peptide, recombinant human IFITM1, recombinant human IFITM2 and recombinant human IFITM3 were used in the ELISA test. Results were expressed in O.D. means. **C-** The monoclonal antibody 5D11B9 was tested for binding to Vero E6 and Calu-3 cell surfaces by flow cytometry. The results showed mAb signal titration from 80 µg/ml to 5 µg/ml as the mean percentage of positive cells (error bars indicate S.D.). **D-** Calu-3 cells were seeded on glass coverslips, processed for immunofluorescence and analyzed by confocal imaging. Merged images show DAPI staining of DNA (blue) and IFITM2 (red). Scale bars: 5 µm.

(Fig. S2- panel A) and with specific IFITM2 siRNAs (Fig. S2- panel B–C).

3.2. The 5D11B9 anti-IFITM2 mAb inhibits SARS-CoV-2 Spike internalization

To verify the reported involvement of IFITM2 in the SARS-CoV-2 cell entry process mediated by the binding of the viral Spike protein to the ACE2 receptor (Li et al., 2003), the effects of 5D11B9 mAb treatment on the Spike binding to the cells was investigated. A neutralizing serum obtained from a SARS-CoV-2-convalescent patient efficiently prevented the Spike binding onto the cell surface, whereas 5D11B9 mAb increased the binding signal (Fig. 2A), thus indicating the accumulation of S-protein on the cell surface and suggesting the contemporary blockade of the internalization process. Further evidence supporting this hypothesis was obtained by confocal microscopy in Calu-3 cells (Fig. 2B). Spike signals appear on the cell membrane after 5 min incubation and move towards the cell cytoplasm as soon as S-protein is internalized in about 30 min (Fig. 2B, right column: unrelated murine mAb treatment). In contrast, the addition of the 5D11B9 mAb does not allow S-protein to move into the cytoplasm, as shown by the unaltered signal localization onto the cell surface after 30 min (Fig. 2B, left column). Moreover, the impairing effects of 5D11B9 anti-IFITM2 mAb treatment on S-protein trafficking was showed by Proximity-Ligation Assay performed between Spike and ACE2 (cell surface localization) or Rab5a (endosomal localization) (Prelli Bozzo et al., 2021). The assay allowed to confirm Spike and ACE2 proximity 5 min after mouse Fc-tagged Spike treatment of Calu-3 cells, and contemporary no PLA signal with the endosomal marker Rab5a. After 30 min, the increased PLA signal with Rab5a showed that Spike protein was internalized in endosomes (Fig. 2C–D). At the same time point, the treatment with the 5D11B9 anti-IFITM2 mAb reduced the colocalization of S-protein with Rab5, as demonstrated by the decrease of about 50% of the Rab5a PLA signal, and the equivalent signal persistence of the ACE2 PLA signal related to the Spike membrane localization. These pieces of evidence let infer that the 5D11B9 mAb can impair Spike internalization (Fig. 2C–D), while having no effect on ACE2 enzymatic activity (Fig. S3).

3.3. Viral yield is highly reduced in cultures infected with SARS-CoV-2 in the presence of 5D11B9 anti-IFITM2 mAb

Calu-3 cells were used to determine whether the 5D11B9 mAb also affects viral replication and the yield of infectious virus particles. Indeed, RT-PCR analysis of mRNA from Calu-3 cells infected with SARS-CoV-2 in the presence of 5D11B9 mAb revealed a significantly decreased expression of the N and Spike (S) genes (10^2 and 10^4- fold reduction, respectively) when compared with cells infected in the presence of a control unrelated murine mAb (Fig. 3A–B). Calu-3 supernatants from the experiment shown in Fig. 3A–B, were used in a yield reduction assay on Vero E6 cells. The results show that a 30 µg/ml dose of 5D11B9 mAb can significantly ($p < 0.001$) reduce the viral titer by about two orders of magnitude (100x), thus confirming that the inhibitory effect of 5D11B9 mAb on virus entry results into a strikingly reduction of the viral cytopathic effect (Fig. 3C). Similar results were also obtained by infecting cells with the Omicron BA.1 variant (Fig. 3D). Thus the inhibition of 5D11B9 mAb on Spike-mediated membrane fusion is effective in reducing SARS-CoV-2 infection, and does not show toxic effects on cell viability (Fig. 3E), neither induces cell apoptosis/necrosis in freshly isolated peripheral mononuclear blood cells (Fig. 3F). Furthermore, the

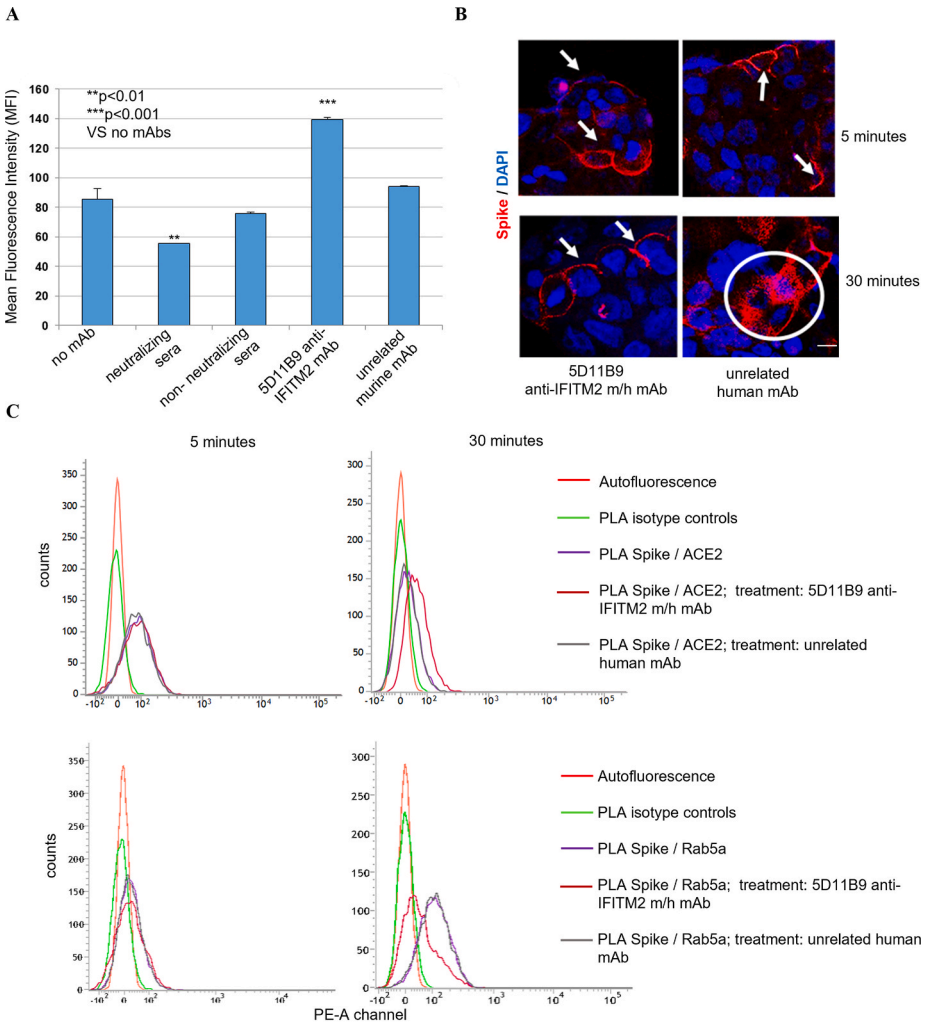

Fig. 2. Inhibition of Spike protein internalization in host cells by the 5D11B9 anti-IFITM2 mAb.
A- Flow cytometry assays were performed to test the binding of the recombinant biotinylated Spike protein to the Vero E6 cell surface using a PE-conjugated streptavidin. A human-neutralizing and a non-neutralizing sera (1:30 dilution) were used as positive and negative controls, respectively. The 5D11B9 mAb was added at a concentration of 30 μg/ml. The graph shows the results as Mean Fluorescent Intensity (error bars indicate S.D.). A two-tailed *t*-test was performed between the indicated groups. **B-** Calu-3 cells were treated with a mouse Fc-tagged SARS-CoV-2 S1 spike recombinant protein (5 μg/ml) in the presence of the recombinant 5D11B9 anti-IFITM2 m/h chimera mAb or an unrelated recombinant human mAb (15 μg/ml) for 1 h at 4 °C. Cells were then incubated at 37 °C and harvested after 5 and 30 min, and the signal from the spike protein was detected by immunofluorescence and confocal microscopy acquisition. The arrows in the figure refer to Spike protein associated with the plasma membrane, while the circle indicates spike protein signal diffusion in the cytoplasm. Merged images show DNA staining with DAPI (blue) and mouse Fc-tagged SARS-CoV-2 S1 spike recombinant protein (red). Scale bar: 5 μm. **C-** Calu-3 cells were treated with a mouse Fc-tagged SARS-CoV-2 S1 spike recombinant protein in the presence of a recombinant 5D11B9 m/h chimera or an unrelated recombinant human mAb for 1 h at 4 °C. Cells were then incubated at 37 °C and harvested after 5 and 30 min. (UP) PLA signal between Spike and ACE-2 after 5 and 30 min at 37 °C. (DOWN) PLA signal between Spike and Rab5a after 5 and 30 min at 37 °C. Graphs depict the signal overlays in the described experimental conditions. **D-** Data obtained from 30 min incubation were displayed in a table as Mean Fluorescent Intensity (error bars indicate S.D.). A two-tailed *t*-test was performed between the indicated groups.

D

	no mAb (MFI ± S.D.)	**5D11B9 anti-IFITM2 m/h mAb** (MFI ± S.D.)	**unrelated human mAb** (MFI ± S.D.)
no PLA	2.50 ± 0.70		
PLA: isotype controls	12.50 ± 0.70		
PLA: Spike/ACE2	36.50 ± 0.70	69.00 ± 1.41 *	36.00 ±0.00
PLA: Spike/Rab5a	119.00 ± 2.80	66.5 ± 2.12 *	117.00 ± 0.00

*p<0.01 VS no mAb
P<0.001 Vs unrelated human mAb

inhibition of the viral cytopathic effect and the performance of 5D11B9 mAb was also confirmed by the positive results obtained in comparative assays with other commercially available anti-IFITM2 Abs (Fig. S4). Spike-mediated membrane fusion is also responsible for syncytia formation, a major morphological signature in SARS-CoV-2 damaged lungs (Rajah et al., 2022). The effect of 5D11B9 mAb on the formation of Spike-induced cell syncytia was investigated by GFP split assay (Buchrieser et al., 2020). Spike-expressing donor cells were allowed to fuse with acceptor cells (endogenously expressing ACE2) (Fig. 4A) and after 24 h GFP-positive syncytia were analyzed. Fig. 4B shows a representative image of GFP-positive syncytia obtained in Vero E6 cells, where cultures treated with the 5D11B9 mAb displayed a lower positive signal. Flow cytometry was used to measure the percentage of GFP-positive cells both in Vero E6 and Calu-3 cells. As shown in Figs. 4C, 5D11B9 anti-IFITM2 mAb was able to reduce the number of syncytia in a dose-dependent manner. It is worth noting that a higher efficacy was observed in human Calu-3 cells compared to Vero E6 monkey cells, probably due to the structural difference of 3 out of 10 amino acids in the mAb epitope in monkey and human proteins, but probably also due to the different expression of specific proteases involved in the entry pathways of the two analyzed cells types (Shang et al., 2020).

3.4. The 5D11B9 anti-IFITM2 mAb inhibits HSVs- and RSV-induced cytopathic effects

In order to investigate the possibility that the 5D11B9 anti-IFITM2 mAb could also impair cell entry by other viruses, we analyzed the effect of the mAb on HSVs- and RSV- replication. To this end, Vero E6 cells and human HSVs-permissive HeLa cells were infected with HSV-1 or HSV-2, and the inhibition of the viral cytopathic effect was evaluated in relation to the number of formed plaques. Notably, treatments with 30 μg/ml of the 5D11B9 mAb reduced by approximately 55% the numbers of HSVs-induced plaques in Vero E6 cells (Fig. 5A), while a more striking result was observed in human HeLa cells, where the mAb reduced by about 70% and 40% the number of plaques induced by HSVs at 30 and 3 μg/ml, respectively (Fig. 5B). This result suggests, once again, a higher reactivity of the 5D11B9 mAb with the human epitope. The antiviral efficacy of the 5D11B9 mAb was finally tested in the RSV- permissive

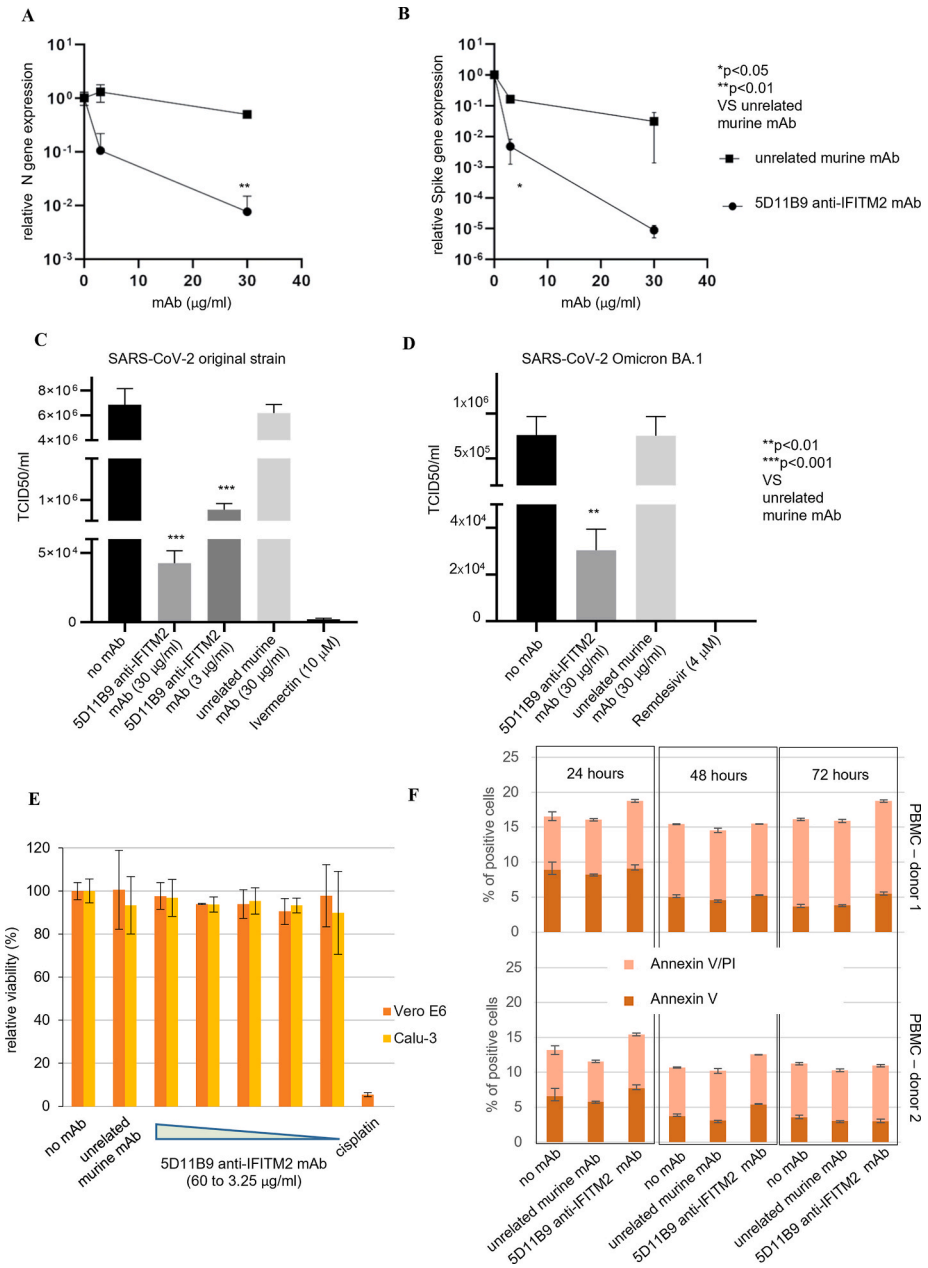

Fig. 3. Reduction of viral yield in cells infected with SARS-CoV-2 in the presence of the 5D11B9 anti-IFITM2 mAb.

A, B- Calu-3 cells were plated into 12-well plates (2 × 10^5 cells/well) in culture medium. The next day, the monolayer was treated with the 5D11B9 anti-IFITM2 mAb or with an unrelated murine mAb (30 μg/ml or 3 μg/ml) and contemporarily with SARS-CoV-2 (MOI 0.01) at 37 °C for 2 h. After 48 h, total RNA was obtained and used for Nucleocapsid, Spike and GAPDH gene detection in cultures (supernatants + cells). Graphs depict means (+SD) calculated as S and N gene relative expression using the $2^{-\Delta\Delta Ct}$ method. GAPDH gene expression was used to normalize RNA level content. **C-** Calu-3 cells were infected with SARS-CoV-2 original strain (100 TCID50). The infected cultures were treated with the 5D11B9 anti-IFITM2 mAb at the indicated doses (30 and 3 μg/ml) or with an unrelated murine mAb. Ivermectin (10 μM) was used as positive control. Viral yields in the culture supernatant were determined by titration on Vero E6 cells on day 2 post-infection and reported as TCID50/ml (mean ± SD). A two-tailed *t*-test was performed between the indicated groups. **D-** Human Calu-3 cells were infected with Omicron BA.1 variant (100 TCID50). Cultures were treated with 5D11B9 mAb or with an unrelated murine mAb. Remdesivir (4 μM) was used as positive control. Viral yields in the culture supernatant were determined by titration on day 5 post-infection and reported as TCID50/ml (mean ± SD). A two-tailed *t*-test was performed between the indicated groups. **E-** Vero E6 and Calu-3 cells were cultured in 96-well plates and treated with different concentrations of monoclonal antibody 5D11B9 (80, 40, 20, 10 and 5 μg/ml) or with an unrelated murine IgG2b (60 μg/ml). After 48 h of incubation, cells were analyzed by CCK-8 cell viability assay. Data was obtained from triplicate samples. The results are shown as the percentage (%) of viable cells with respect to control. **F-** PBMCs from two healthy donors were plated in 24-well plates (1 × 10^6 cells/ml) in culture medium and treated with the monoclonal antibody 5D11B9 (40 μg/ml) or with an unrelated murine IgG2b (40 μg/ml). At the indicated time points (24, 48, 72 h) apoptotic cells were determined by FACS by using FITC Annexin V with propidium iodide. The results are shown as the percentage (%) of Annexin V/PI positive cells.

human HEp-2 cell line (Fig. 5C). A yield reduction assay on Vero E6 cells was performed in the supernatants from human HEp-2 cells infected with genuine RSV in the presence of the 5D11B9 mAb, or 6-azauridine used as a positive control. Notably, a 30 μg/ml dose of 5D11B9 mAb appeared to reduce by about two orders of magnitude (100x) the viral yield.

4. Discussion

IFITM proteins constitute a family of molecules for which opposing effects on virus infection have been reported (Prelli Bozzo et al., 2022) and whose study has recently unveiled their involvement with SARS-CoV-2 infection. In fact, the antiviral properties of IFITM1, IFITM2 and IFITM3 are undoubted, mostly related to the restriction of host cell penetration of several viruses (Zhao et al., 2019). This restriction has been suggested to rely on IFITMs ability to alter the mechanical properties of cellular membranes, disfavoring the membrane fusion reaction between the virus and the target cell. On the other hand, this mechanism does not appear to concern the generality of viruses, as several of them are known to be resistant to IFITM-mediated restriction (Majdoul and Compton, 2021). Finally, recent evidence has indicated that IFITMs can exert not an inhibitory, but a promoting activity on SARS-CoV-2 entry into the host cell and that the virus hijacks them for efficient viral infection (Prelli Bozzo et al., 2021; 2022). The findings here reported, deepen the knowledge about the IFITM2-mediated regulation of cell infection by pathogenic viruses, and the use of an IFITM2-specific mAb confirms the singular function of this IFITM family member in facilitating SARS-CoV-2 cell infection.

The anti-infective approach suggested in this study challenges the traditional idea that pharmacological targets should be sought out first at the infectious agent rather than at the cellular determinants/mechanisms that permits the completion of the infection process. Indeed, the availability of host-directed therapeutics for infectious diseases could be more resilient to the obsolescence deriving from the inherent phenotypic diversity of viral targets. A significant number of authorized antibodies for SARS–CoV-2 therapy, as well as other developing antibodies have

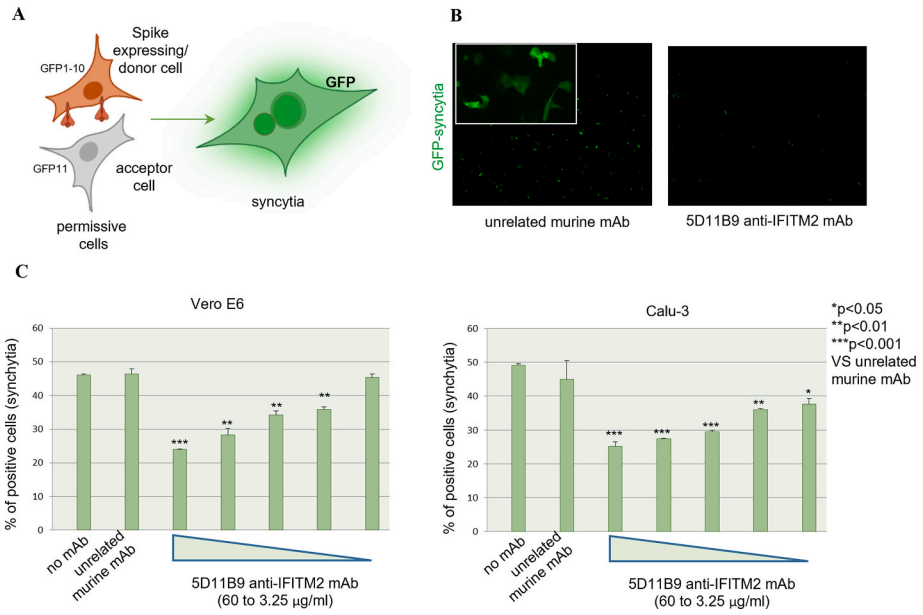

Fig. 4. Reduction of SARS-CoV-2- induced cells syncytia in the presence of the 5D11B9 anti-IFITM2 mAb.

A- Picture displaying the GFP-split (syncytia formation) assay developed in Vero E6 and Calu-3 cells. **B-** Representative images of GFP positive syncytia in Vero E6 cells treated with the anti-IFITM2 specific mAb or an unrelated murine mAb. Images are obtained by using 5× magnification. The upper left insert was obtained by using 20× magnification and shows the appearance of multinucleated GFP- positive cells. **C-** Vero E6 (left graph) or Calu-3 (right graph) were transfected with GFP1-10 and Spike or with GFP11 in suspension at 37 °C, shaking at 900 rpm for 30 min. After transfection, cells were washed, resuspended in complete medium, and mixed at a 1:1 ratio. After 8 h, the cells were incubated with different concentrations (60, 30, 15, 7.5, and 3.25 µg/ml) of the 5D11B9 anti-IFITM2 mAb or with an unrelated murine mAb (60 µg/ml). The following day, at 24 h post-transfection syncytia formation was quantified by flow cytometry and expressed as the mean percentage (%) of positive cells (syncytia). Error bars indicated S.D. and a two-tailed *t*-test was performed between the indicated groups.

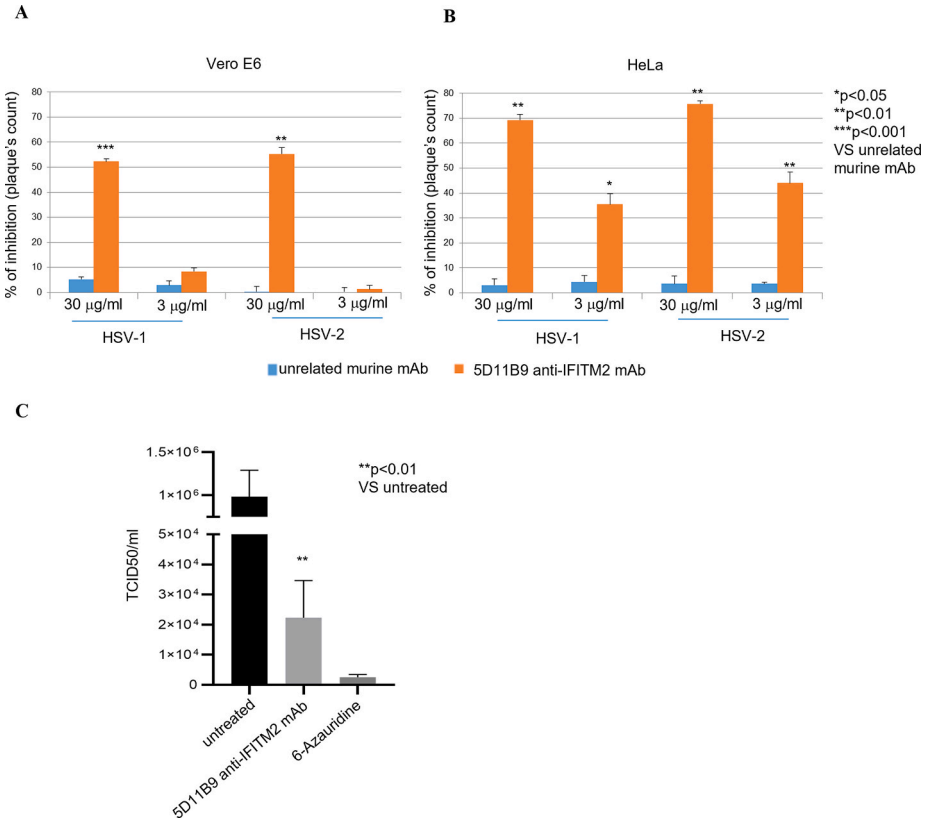

Fig. 5. Inhibition of HSVs- and RSV- cytopathic effects by the 5D11B9 anti-IFITM2 mAb.

A, B- Vero E6 or HeLa cells were plated in 12-well cell culture plates (2×10^5 cells/well) in culture medium. The next day, the monolayer was treated with the 5D11B9 anti-IFITM2 mAb or an unrelated murine mAb (30 or 3 µg/ml) and simultaneously infected with HSV-1 or HSV-2. Two hours post-infection, cells were washed with PBS 1X and overlaid with carboxymethylcellulose 0.5% mixed with Dulbecco's Modified Eagle's Medium (DMEM). After 48h, the cytopathic effect is first observed under the microscope and stained with Crystal Violet 0.5%/ Formaldehyde 4%. The results are shown as percentage (%) of inhibition of plaque formation (error bars indicate S.D.) and a two-tailed *t*-test was performed between the indicated groups. **C-** HEp-2 cells were infected with RSV (100 TCID50). The infected cultures were treated with the 5D11B9 anti-IFITM2 mAb at a concentration of 30 µg/ml 6-Azauridine (4 µM) was used as an internal control. Viral yields in the culture supernatant were determined by titration in Vero E6 cells on day 4 post-infection and reported as TCID50/ml. Data are expressed as mean (error bars indicate S.D.) and a two-tailed *t*-test was performed between the indicated groups.

become ineffective at the emergence and spread of the Omicron variants (Fang, 2022). This reversal of perspective is often difficult or impossible to pursue, since cellular targets and the interference with the processes they regulate entail risks and side effects that are unacceptable and intolerable. Even in the case of SARS-CoV-2 it would be risky to envisage the use of drugs directed against the membrane protein ACE2, since its angiotensin converting activity regulates blood pressure with protective functions for the cardiovascular system and other organs (Verano-Braga et al., 2020). On the other hand, we report that IFITM2, although involved in the interaction with the Spike/ACE2 complex, can be bound by a selective mAb without altering the ACE2 enzymatic activity. Moreover, besides the involvement in innate immunity (Yánez et al., 2019) or in cancer-related signaling (Rosati et al., 2015), no further cellular functions, to date, has been associated with IFITM2 protein (Friedlová et al., 2022). These pieces of evidence lay the foundations of a hopefully successful, cheaper, and broader spectrum antiviral approach as an alternative or complement to the efforts of a great part of the current industrial investment focused on the production of neutralizing

anti-Spike monoclonal antibodies, whose efficacy could be affected by the protein changing in emerging viral variants. Conversely, as above noted for cellular targets, IFITM2 is not subject to rapid structural variability.

5. Conclusions

The here suggested IFITM2 specific targeting could be a more robust and broadly applicable tool for SARS-CoV-2 variants, as well as other viruses exploiting the IFITM2 docking mechanism on the plasma membrane to bind and enter into the host cell. The identification of a pharmacological tool directed against a cellular determinant that regulates the first stages of viral adhesion and invasion is also proposed as a useful aid for early or preventive treatment in all emerging viral pathologies, or those not yet sufficiently characterized, sensitive to the mechanism of inhibition mediated by the neutralization of the IFITM2 protein.

Author contributions

AR, LM, and MCT designed the studies. AB, CZ, GS, GF, MG, AR, and LM conducted experiments and acquired data. MC, MDM, and AR cured data presentation. AB, MDM, AR, and LM performed statistical analysis. AR, GF, MG, MCT, VDL, AM, and LM contributed to manuscript writing and editing.

Declaration of competing interest

The authors declare the following financial interests/personal relationships which may be considered as potential competing interests: Shareholders of the academic spin-off FIBROSYS s.r.l., which has filed a patent application relating to this work, include AR, MDM, MCT, VDL and LM. The other authors have nothing to declare.

Data availability

Data will be made available on request.

Acknowledgements

This study was supported by: University of Salerno Intramural Funds (FARB) to LM; PRIN 2017 “Natural and pharmacological inhibition of the early phase of viral replication (VirSudNet)” N° 2017M8R7N9 to AM and the VALERE project funded by the University of Campania “Luigi Vanvitelli” to MG. Authors also thank Prof. Frank Kirchhoff and Dr. Rayahne Nchioua from the Institute of Molecular Virology (Ulm University Medical Center) and Prof. Rino Rappuoli, Dr. Emanuele Andreano and Dr. Ida Paciello from Fondazione Toscana Life Sciences for helpful discussions and meaningful suggestions during manuscript preparation.

Appendix A. Supplementary data

Supplementary data to this article can be found online at https://doi.org/10.1016/j.antiviral.2023.105546.

References

Baggen, J., Vanstreels, E., Jansen, S., Daelemans, D., 2021. Cellular host factors for SARS-CoV-2 infection. Nat. Microbio. 6, 1219–1232. https://doi.org/10.1038/s41564-021-00958-0.

Bailey, C.C., Kondur, H.R., Huang, I.-C., Farzan, M., 2013. Interferon-induced transmembrane protein 3 is a type II transmembrane protein. J. Biol. Chem. 288, 32184–32193. https://doi.org/10.1074/jbc.m113.514356.

Brass, A.L., Huang, I.-C., Benita, Y., John, S.P., Krishnan, M.N., Feeley, E.M., Ryan, B.J., Weyer, J.L., van der Weyden, L., Fikrig, E., Adams, D.J., Xavier, R.J., Farzan, M., Elledge, S.J., 2009. The IFITM proteins mediate cellular resistance to Influenza A H1N1 virus, west nile virus, and dengue virus. Cell 139, 1243–1254. https://doi.org/10.1016/j.cell.2009.12.017.

Buchrieser, J., Dufloo, J., Hubert, M., Monel, B., Planas, D., Rajah, M.M., Planchais, C., Porrot, F., Guivel-Benhassine, F., Van der Werf, S., Casartelli, N., Mouquet, H., Bruel, T., Schwartz, O., 2020. Syncytia formation by SARS-CoV-2-infected cells. EMBO J. 39 https://doi.org/10.15252/embj.2020106267.

Chew, K.W., Moser, C., Daar, E.S., Wohl, D.A., Li, J.Z., Coombs, R.W., Ritz, J., Giganti, M., Javan, A.C., Li, Y., Choudhary, M.C., Deo, R., Malvestutto, C., Klekotka, P., Price, K., Nirula, A., Fischer, W., Bala, V., Ribeiro, R.M., Perelson, A.S., Fletcher, C.V., Eron, J.J., Currier, J.S., Hughes, M.D., Smith, D.M., 2022. Antiviral and clinical activity of bamlanivimab in a randomized trial of non-hospitalized adults with COVID-19. Nat. Commun. 13 https://doi.org/10.1038/s41467-022-32551-2.

Fang, F.F., 2022. As the virus evolves, so too must we: a drug developer’s perspective : we need a new paradigm in searching for next-generation countermeasures. Virol J 10 19 (1), 159. https://doi.org/10.1186/s12985-022-01887-y (Fa).

Fiolet, T., Kherabi, Y., MacDonald, C.-J., Ghosn, J., Peiffer-Smadja, N., 2022. Comparing COVID-19 vaccines for their characteristics, efficacy and effectiveness against SARS-CoV-2 and variants of concern: a narrative review. Clin. Microbiol. Infect. 28, 202–221. https://doi.org/10.1016/j.cmi.2021.10.005.

Forster, P., Forster, L., Renfrew, C., Forster, M., 2020. Phylogenetic network analysis of SARS-CoV-2 genomes. Proc. Natl. Acad. Sci. USA 117, 9241–9243. https://doi.org/10.1073/pnas.2004999117.

Friedlová, N., Zavadil Kokáš, F., Hupp, T.R., Vojtěšek, B., Nekulová, M., 2022. IFITM protein regulation and functions: Far beyond the fight against viruses. Front. Immunol. 13, e1042368 https://doi.org/10.3389/fimmu.2022.1042368.

Galloway, S.E., Paul, P., MacCannell, D.R., Johansson, M.A., Brooks, J.T., MacNeil, A., Slayton, R.B., Tong, S., Silk, B.J., Armstrong, G.L., Biggerstaff, M., Dugan, V.G., 2021. Emergence of SARS-CoV-2 B.1.1.7 lineage — United States, december 29, 2020–january 12, 2021. MMWR. Morbidity and Mortality Weekly Report 70, 95–99. https://doi.org/10.15585/mmwr.mm7003e2.

Huang, I.-C., Bailey, C.C., Weyer, J.L., Radoshitzky, S.R., Becker, M.M., Chiang, J.J., Brass, A.L., Ahmed, A.A., Chi, X., Dong, L., Longobardi, L.E., Boltz, D., Kuhn, J.H., Elledge, S.J., Bavari, S., Denison, M.R., Choe, H., Farzan, M., 2011. Distinct patterns of IFITM-mediated restriction of filoviruses, SARS coronavirus, and Influenza A virus. PLoS Pathog. 7, e1001258 https://doi.org/10.1371/journal.ppat.1001258.

Jackson, C.B., Farzan, M., Chen, B., Choe, H., 2021. Mechanisms of SARS-CoV-2 entry into cells. Nat. Rev. Mol. Cell Biol. 23, 3–20. https://doi.org/10.1038/s41580-021-00418-x.

Korber, B., Fischer, W.M., Gnanakaran, S., Yoon, H., Theiler, J., Abfalterer, W., Hengartner, N., Giorgi, E.E., Bhattacharya, T., Foley, B., Hastie, K.M., Parker, M.D., Partridge, D.G., Evans, C.M., Freeman, T.M., de Silva, T.I., McDanal, C., Perez, L.G., Tang, H., Moon-Walker, A., Whelan, S.P., LaBranche, C.C., Saphire, E.O., Montefiori, D.C., Angyal, A., Brown, R.L., Carrilero, L., Green, L.R., Groves, D.C., Johnson, K.J., Keeley, A.J., Lindsey, B.B., Parsons, P.J., Raza, M., Rowland-Jones, S., Smith, N., Tucker, R.M., Wang, D., Wyles, M.D., 2020. Tracking changes in SARS-CoV-2 spike: evidence that D614G increases infectivity of the COVID-19 virus. Cell 182, 812–827. https://doi.org/10.1016/j.cell.2020.06.043 e19.

Ledford, H., 2022a. The next variant: three key questions about what’s after Omicron. Nature 603, 212–213. https://doi.org/10.1038/d41586-022-00510-y.

Ledford, H., 2022b. Hundreds of COVID trials could provide a deluge of new drugs. Nature 603, 25–27. https://doi.org/10.1038/d41586-022-00562-0.

Lee, J.Y., Wing, P.A., Gala, D.S., Noerenberg, M., Järvelin, A.I., Titlow, J., Zhuang, X., Palmalux, N., Iselin, L., Thompson, M.K., Parton, R.M., Prange-Barczynska, M., Wainman, A., Salguero, F.J., Bishop, T., Agranoff, D., James, W., Castello, A., McKeating, J.A., Davis, I., 2022. Absolute quantitation of individual SARS-CoV-2 RNA molecules provides a new paradigm for infection dynamics and variant differences. Elife 11. https://doi.org/10.7554/elife.74153.

Li, W., Moore, M.J., Vasilieva, N., Sui, J., Wong, S.K., Berne, M.A., Somasundaran, M., Sullivan, J.L., Luzuriaga, K., Greenough, T.C., Choe, H., Farzan, M., 2003. Angiotensin-converting enzyme 2 is a functional receptor for the SARS coronavirus. Nature 426, 450–454. https://doi.org/10.1038/nature02145.

Majdoul, S., Compton, A.A., 2021. Lessons in self-defence: inhibition of virus entry by intrinsic immunity. Nat. Rev. Immunol. 22, 339–352. https://doi.org/10.1038/s41577-021-00626-8.

Mulder, N., 2022. Faculty Opinions recommendation of Whole genome sequencing reveals host factors underlying critical Covid-19. Faculty Opin. – Post-Publ. Peer Review Biomed. Lit. https://doi.org/10.3410/f.741781629.793592206.

Nchioua, R., Schundner, A., Kmiec, D., Prelli Bozzo, C., Zech, F., Koepke, L., Graf, A., Krebs, S., Blum, H., Frick, M., Sparrer, K.M.J., Kirchhoff, F., 2022. SARS-CoV-2 variants of concern hijack IFITM2 for efficient replication in human lung cells. J. Virol. 96 https://doi.org/10.1128/jvi.00594-22.

Prelli Bozzo, C., Kmiec, D., Kirchhoff, F., 2022. When good turns bad: how viruses exploit innate immunity factors. Curr. Opin. Virol. 52, 60–67. https://doi.org/10.1016/j.coviro.2021.11.009.

Prelli Bozzo, C., Nchioua, R., Volcic, M., Koepke, L., Krüger, J., Schütz, D., Heller, S., Stürzel, C.M., Kmiec, D., Conzelmann, C., Müller, J., Zech, F., Braun, E., Groß, R., Wettstein, L., Weil, T., Weiß, J., Diofano, F., Rodríguez Alfonso, A.A., Wiese, S., Sauter, D., Münch, J., Goffinet, C., Catanese, A., Schön, M., Boeckers, T.M., Stenger, S., Sato, K., Just, S., Kleger, A., Sparrer, K.M.J., Kirchhoff, F., 2021. IFITM proteins promote SARS-CoV-2 infection and are targets for virus inhibition in vitro. Nat. Commun. 12 https://doi.org/10.1038/s41467-021-24817-y.

Rajah, M.M., Bernier, A., Buchrieser, J., Schwartz, O., 2022. The mechanism and consequences of SARS-CoV-2 spike-mediated fusion and syncytia formation. J. Mol. Biol. 434, 167280 https://doi.org/10.1016/j.jmb.2021.167280.

Rosati, A., Basile, A., D'Auria, R., d'Avenia, M., De Marco, M., Falco, A., Festa, M., Guerriero, L., Iorio, V., Parente, R., Pascale, M., Marzullo, L., Franco, R., Arra, C., Barbieri, A., Rea, D., Menichini, G., Hahne, M., Bijlsma, M., Barcaroli, D., Sala, G., di Mola, F.F., di Sebastiano, P., Todoric, J., Antonucci, L., Corvest, V., Jawhari, A., Firpo, M.A., Tuveson, D.A., Capunzo, M., Karin, M., De Laurenzi, V., Turco, M.C., 2015. BAG3 promotes pancreatic ductal adenocarcinoma growth by activating stromal macrophages. Nat. Commun. 6 https://doi.org/10.1038/ncomms9695.

Shang, J., Wan, Y., Luo, C., Ye, G., Geng, Q., Auerbach, A., Li, F., 2020. Cell entry mechanisms of SARS-CoV-2. Proc. Natl. Acad. Sci. USA 117, 11727–11734. https://doi.org/10.1073/pnas.2003138117.

Sun, F., Xia, Z., Han, Y., Gao, M., Wang, L., Wu, Y., Sabatier, J.M., Miao, L., Cao, Z., 2020. Topology, Antiviral Functional Residues and Mechanism of IFITM1. Viruses. 12 (3), 295. https://doi.org/10.3390/v12030295, 8.

Van Kerkhove, M.D., 2021. COVID-19 in 2022: controlling the pandemic is within our grasp. Nat. Med. 27 https://doi.org/10.1038/s41591-021-01616-y, 2070–2070.

Verano-Braga, T., Martins, A.L.V., Motta-Santos, D., Campagnole-Santos, M.J., Santos, R. A.S., 2020. ACE2 in the renin–angiotensin system. Clin. Sci. 134, 3063–3078. https://doi.org/10.1042/cs20200478.

Weston, S., Czieso, S., White, I.J., Smith, S.E., Kellam, P., Marsh, M., 2014. A membrane topology model for human interferon inducible transmembrane protein 1. PLoS One 9 (8), e104341. https://doi.org/10.1371/journal.pone.0104341, 8.

Yánez, D.C., Ross, S., Crompton, T., 2019. The IFITM protein family in adaptive immunity. Immunology 159, 365–372. https://doi.org/10.1111/imm.13163.

Zannella, C., Giugliano, R., Chianese, A., Buonocore, C., Vitale, G.A., Sanna, G., Sarno, F., Manzin, A., Nebbioso, A., Termolino, P., Altucci, L., Galdiero, M., de Pascale, D., Franci, G., 2021. Antiviral activity of Vitis vinifera leaf extract against SARS-CoV-2 and HSV-1. Viruses 13, 1263. https://doi.org/10.3390/v13071263.

Zhao, X., Li, J., Winkler, C.A., An, P., Guo, J.-T., 2019. IFITM genes, variants, and their roles in the control and pathogenesis of viral infections. Front. Microbiol. 9 https://doi.org/10.3389/fmicb.2018.03228.